



HAL
open science

Optimal cavity shape design for acoustic liners using Helmholtz equation with visco-thermal losses

Gilles Tissot, Gwenael Gabard

► **To cite this version:**

Gilles Tissot, Gwenael Gabard. Optimal cavity shape design for acoustic liners using Helmholtz equation with visco-thermal losses. *Aeroacoustics 2019 - 25th AIAA/CEAS Aeroacoustics Conference*, May 2019, Delft, Netherlands. pp.1-11, 10.2514/6.2019-2471 . hal-02335834

HAL Id: hal-02335834

<https://inria.hal.science/hal-02335834>

Submitted on 28 Oct 2019

HAL is a multi-disciplinary open access archive for the deposit and dissemination of scientific research documents, whether they are published or not. The documents may come from teaching and research institutions in France or abroad, or from public or private research centers.

L'archive ouverte pluridisciplinaire **HAL**, est destinée au dépôt et à la diffusion de documents scientifiques de niveau recherche, publiés ou non, émanant des établissements d'enseignement et de recherche français ou étrangers, des laboratoires publics ou privés.

Optimal cavity shape design for acoustic liners using Helmholtz equation with visco-thermal losses

Gilles TISSOT^{1,2} and Gwénaél GABARD²

¹*INRIA Rennes Bretagne Atlantique, IRMAR – UMR CNRS 6625, av. Général Leclerc, 35042 Rennes, France*

²*Laboratoire d'Acoustique de l'Université du Mans, av. Olivier Messiaen, 72085 Le Mans, France*

This paper presents a shape optimisation strategy to design a cavity for acoustic liners, that approaches at best a target impedance over a given frequency range, penalising too large shape displacements from an initial guess. A model based on the Helmholtz equation is used, where the visco-thermal losses are taken into account by an equivalent impedance boundary condition. Using an adjoint-based method, the gradient of the cost functional with respect to shape variations is calculated, and regularised by a Sobolev gradient. A finite element method is employed with XFEM cut elements, that allows to consider an immersed boundary which is localised by a level-set function. We show that with this method, we are able to obtain a cavity shape leading to an almost perfect absorption for a frequency in the prescribed optimisation range.

I. Introduction

Acoustic liners is a technology currently integrated in nacelles of aircraft engines in order to absorb noise coming from the fan or the combustion chamber. Constraints on treatment size, weight, and frequency range become extremely restrictive, especially when the trend is the design of higher dilution rate engines. Indeed, in that case, the noise is shifted toward low frequencies, requiring thicker liners, while in contrary thinner treatments are desired. The standard single-degree-of-freedom liners are composed of a honeycomb structure covered by a perforated plate. The principle is to generate a resonance in the cavity, that induces large velocities through the perforations, where viscous dissipations take place, resulting in sound absorption. The context of the present study is to search for optimal cavity shapes in order to absorb as much as possible at low frequencies. We adopt then a strategy of shape optimisation.

Shape optimisation has become popular in various domains, such as in elasticity [1–5], aerodynamics [6, 7] or optics [8, 9]. In acoustics some studies were performed, mainly to find optimal horns [10–14], to optimize Helmholtz resonators [15] or for room acoustics [16, 17]. In acoustics, the use of the Helmholtz equation is convenient for its simplicity and its relatively low numerical cost. However, it neglects viscous losses and doesn't allow for the exploration of the absorption mechanisms. On the other hand, the use of the full linearised Navier–Stokes equations, as in Caeiro et al. [15], can become extremely expensive in terms of numerical costs. We propose in the present study to develop a shape optimisation strategy with the model introduced by Berggren et al. [18], that is a Helmholtz-like equation with a model of losses. This model is similar to the study of Bossart et al. [19] and assumes that most of the visco-thermal losses take place within the acoustic boundary layer. Based on an integral across the acoustic boundary layer, and assuming that it is infinitely thin with small wall curvatures, it leads to an equivalent impedance boundary condition mimicking the visco-thermal losses.

A recent study of Andersen et al. [20] handles a similar objective than the present paper optimising Helmholtz resonators for maximising the absorption coefficients but for a transmission problem and not in normal incidence. Their approach is complementary compared to our study since they use a BEM formulation and the shape is parametrised by cubic splines and a single frequency is targeted, while we don't assume any parametrisation due to the XFEM formulation.

A common difficulty in shape optimisation is that it can yield shapes that are very efficient, but so complex that they are impossible to manufacture. Inspired by the work of Allaire et al. [21] and the definition of the shape distance function, we propose a Tikhonov regularisation [22] by penalising shape displacements from a given initial guess.

In section II we present the model and we define the variables necessary for the optimisation. In section III we set up the optimisation problem in order to match a target impedance in a given frequency range. We detail how the shape derivative is determined by adjoint method. Moreover, we present the Sobolev gradient regularisation necessary to seek the optimal shape in a class of regular solutions. In section IV the finite element discretisation is presented with

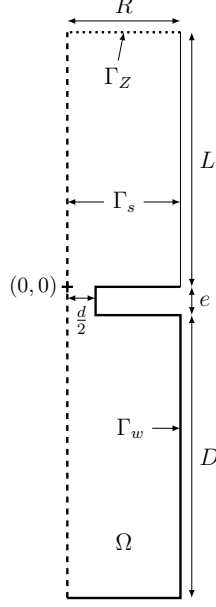


Fig. 1 Schematic representation of the domain.

the XFEM cut elements strategy. We detail the transport and the regularisation of the level set function. Finally in section V, the application of the methodology on the liner problem is presented.

II. Problem formulation

We consider the domain Ω representing a cylindrical cavity with radius R and depth D , a single perforation with diameter d and thickness e and the exterior domain of length L . The geometry is axisymmetric with cylindrical coordinates $x = (r, z)^T$ and $dx = (r dr, dz)^T$. Figure 1 represents the geometry, with Γ_w the wall boundary, Γ_s the free slip boundary and the symmetry axis and Γ_Z the impedance boundary condition where an incoming plane wave is imposed. We define $\Gamma = \Gamma_w \cup \Gamma_s \cup \Gamma_Z$.

We consider the Helmholtz equation in Ω :

$$\begin{cases} \Delta p + k^2 p = 0 & \text{in } \Omega \\ \frac{\partial p}{\partial n} = \delta_v \frac{i-1}{2} \Delta_T p - \delta_T k^2 \frac{(i-1)(\gamma-1)}{2} p & \text{on } \Gamma_w \\ \frac{\partial p}{\partial n} + ikp = 2ike^{ikL} & \text{on } \Gamma_Z \\ \frac{\partial p}{\partial n} = 0 & \text{on } \Gamma_s. \end{cases} \quad (1)$$

where $\mathbf{n}(x)$ the local, outward, unit normal. We consider at the walls (Γ_w) the condition presented in Berggren et al. [18]. This condition assumes that visco-thermal losses are localised in the acoustic boundary layer. It is determined by an integral in the wall-normal direction of the acoustic boundary layer equations. It assumes an infinitely thin boundary layer, and a small wall curvature. In (1)₂, Δ_T is the tangential Laplacian defined such that

$$\Delta p = \Delta_T p + \frac{\partial^2 p}{\partial n^2} + (\nabla_T \cdot \mathbf{n}) \frac{\partial p}{\partial n}. \quad (2)$$

The tangential gradient operator ∇_T is defined such that

$$\nabla p = \nabla_T p + \frac{\partial p}{\partial n} \mathbf{n}. \quad (3)$$

Moreover, we have the viscous and thermal acoustic boundary layer thicknesses

$$\delta_v = \sqrt{\frac{2}{\omega Re_a}} \quad ; \quad \delta_T = \sqrt{\frac{2}{\omega Re_a Pr}}, \quad (4)$$

with Re_a the acoustic Reynolds number and Pr the Prandtl number. An impedance boundary condition is considered for Γ_Z at the entrance of the tube ($y = L$) enforcing an incoming unitary plane wave. We assume the angular frequency $\omega = kc$ to be below the cut-off frequency in the exterior domain, with c the sound speed and k the associated wavenumber.

From the pressure on Γ_Z one can recover the reflection coefficient at $z = 0$:

$$R_f = \left(\bar{p} - e^{ikL} \right) e^{ikL}, \quad (5)$$

with $\bar{p} = \frac{2}{R^2} \int_{\Gamma_Z} p(r, L) r dr$ the average pressure on the boundary $z = L$. The impedance of the treatment at $z = 0$ is then

$$Z = \frac{1 + R_f}{1 - R_f} = \frac{e^{-ikL} - e^{ikL} + \bar{p}}{e^{-ikL} + e^{ikL} - \bar{p}}. \quad (6)$$

III. Optimisation problem

A. Impedance matching

The objective is to modify the shape of the cavity, *i.e.* the domain $\Omega_c = \{x = (r, z) \in \Omega \mid z < 0\}$, in order to match a given target impedance $Z_T(k)$ for a given frequency range $k \in [k_1, k_2]$. We consider the boundary $\Gamma_\theta \subset \Gamma_w$ of Ω_c , that we allow to move during the optimisation, and that will be further modelled by an immersed boundary. We define the cost functional as follows

$$\mathcal{J}(\Omega, p) = \frac{1}{2} \int_{k_1}^{k_2} |Z(k) - Z_T(k)|^2 dk. \quad (7)$$

The problem can be formulated as seeking Ω that minimises (7) under the constraint (1).

To transform this constrained optimisation problem into an unconstrained optimisation problem, we define the Lagrangian

$$\mathcal{L}(\Omega, p, \lambda) = \mathcal{J}(p) - \text{real} \left(\int_{k_1}^{k_2} \left(\lambda, \Delta p + k^2 p \right) dk \right), \quad (8)$$

with $(a, b) = \int_{\Omega} a^* b dx$ and a^* denotes the conjugate of a . λ is the Lagrange multiplier defined to enforce the constraint (1)₁. Other constraints (1)₂ to (1)₄ are enforced by substitution of the boundary terms in the calculations, as it is detailed in VI. Then, we differentiate (8) with respect to each variable (Ω, p, λ) , the corresponding derivatives are equal to zero at the minimum of \mathcal{J} .

The differentiation with respect to λ leads to equation (1)₁, that proves that the constraint is respected when the minimum is reached. The Fréchet derivative with respect to p leads to the following adjoint equation

$$\begin{cases} \Delta \lambda + (k^*)^2 \lambda = 0 & x \in \Omega \\ \frac{\partial \lambda}{\partial n} + \delta_v \frac{i+1}{2} \Delta_T \lambda - \delta_T (k^*)^2 \frac{(i+1)(\gamma-1)}{2} \lambda = 0 & x \in \Gamma_w \\ \frac{\partial \lambda}{\partial n} - ik^* \lambda = \frac{4}{R^2} \frac{e^{ikL} j(p, k)}{\left((e^{-ikL} + e^{ikL} - \bar{p})^2 \right)^*} & x \in \Gamma_Z \\ \frac{\partial \lambda}{\partial n} = 0 & x \in \Gamma_s. \end{cases} \quad (9)$$

The shape sensitivity of \mathcal{J} is determined by vanishing the shape sensitivity of \mathcal{L} , following the formalism presented in Allaire et al. [3]. Let $\delta\theta(x)$ be a smooth displacement direction field of Ω and (f, g) two scalar objective functions. We define the cost functional

$$\mathcal{J}(\Omega) = \int_{\Omega} f(x) dx + \int_{\Gamma} g(x) dx. \quad (10)$$

The shape derivative $\nabla_{\delta\theta}\mathcal{J}$ of the movable boundary Γ_θ , defined in a weak sense by

$$(\nabla_{\delta\theta}\mathcal{J}, \delta\theta.\mathbf{n})_{\Gamma_\theta} = \lim_{\epsilon \rightarrow 0} \frac{\mathcal{J}(\Omega + \epsilon\delta\theta) - \mathcal{J}(\Omega)}{\epsilon} \quad \forall \delta\theta, \quad (11)$$

is equal to

$$(\nabla_{\delta\theta}\mathcal{J}, \delta\theta.\mathbf{n})_{\Gamma_\theta} = \int_{\Gamma_\theta} \delta\theta(x).\mathbf{n}(x) (f(x) + \nabla g.\mathbf{n} + Hg) dx \quad \forall \delta\theta, \quad (12)$$

where H is the local curvature of the boundary $H = \text{div}(\mathbf{n})$. Since shape derivatives involve only quantities at the boundary, the real inner product used to identify the gradient is $(a, b)_{\Gamma_\theta} = \int_{\Gamma_\theta} a b dx$. Moreover only normal shape displacements matter, this is why it is directly introduced in the weak form. In our case, we obtain

$$\begin{aligned} (\nabla_{\delta\theta}\mathcal{L}, \delta\theta.\mathbf{n})_{\Gamma_\theta} &= (\nabla_{\delta\theta}\mathcal{J}, \delta\theta.\mathbf{n})_{\Gamma_\theta} - \int_{k_1}^{k_2} \text{Real} \left[\int_{\Gamma_\theta} (\delta\theta(x).\mathbf{n}(x)) \left(-\nabla\lambda^*.\nabla p + k^2\lambda^*p \right) dx \right] dk \\ &\quad - \int_{k_1}^{k_2} \text{Real} \left[\int_{\Gamma_\theta} (\delta\theta(x).\mathbf{n}(x)) \left(\frac{\partial}{\partial n} \left(\lambda^* \frac{\partial p}{\partial n} \right) + H\lambda^* \frac{\partial p}{\partial n} \right) dx \right] dk = 0. \end{aligned} \quad (13)$$

We assume here that $\Gamma_\theta \subset \Gamma_w$, then $\Gamma_\theta \cap \Gamma_Z = 0$, that means that we are only modifying the shape of the wall. We can note that due to the viscous model, the term $\frac{\partial p}{\partial n}$ does not vanish and the boundary terms should be explicitly computed. We obtain the shape derivative $\nabla_{\delta\theta}\mathcal{J}$

$$\nabla_{\delta\theta}\mathcal{J} = \int_{k_1}^{k_2} \text{Real} \left[\left(-\nabla\lambda^*.\nabla p + k^2\lambda^*p \right) + \left(\frac{\partial}{\partial n} + H \right) \left(-\delta_v \frac{i-1}{2} \nabla_T \lambda^*.\nabla_T p - \delta_T k^2 \frac{(i-1)(\gamma-1)}{2} \lambda^*p \right) \right] dk. \quad (14)$$

B. Regularisation

Shape optimisation suffers intrinsically from the fact that the solution can be arbitrarily complex and then hardly workable. This difficulty can be solved by prescribing an *a priori* shape contour, from which the solution has to be close in a given sense. Thus, we would like to penalise a too large shape variation from the initial domain Ω_0 by Tikhonov regularisation. For that, we define the signed distance function to the initial movable boundary $\Gamma_{\theta,0}$, in a similar manner than in [21],

$$d_{\Omega_0}(x) = \begin{cases} -d(x, \Gamma_{\theta,0}) & \text{if } x \in \Omega_0 \\ 0 & \text{if } x \in \Gamma \\ d(x, \Gamma_{\theta,0}) & \text{if } x \notin \Omega_0, \end{cases} \quad (15)$$

with $d(x, \Gamma)$ the Euclidean distance between x and a boundary Γ :

$$d(x, \Gamma) = \min_{y \in \Gamma} |x - y|. \quad (16)$$

We define the new cost functional regularised by a penalty term as follows

$$\mathcal{J}_r(\Omega, p) = \mathcal{J}(\Omega, p) + \beta \frac{1}{2} \int_{\Gamma_\theta} d_{\Omega_0}^2(x) dx. \quad (17)$$

Remarking that $\nabla d_{\Omega_0}(x) = \mathbf{n}(x)$ on Γ_θ , we can deduce that

$$(\nabla_{\delta\theta}\mathcal{J}_r, \delta\theta.\mathbf{n})_{\Gamma_\theta} = (\nabla_{\delta\theta}\mathcal{J}, \delta\theta.\mathbf{n})_{\Gamma_\theta} + \beta \int_{\Gamma_\theta} (\delta\theta(x).\mathbf{n}(x)) \left(d_{\Omega_0}(x) + H \frac{1}{2} d_{\Omega_0}^2(x) \right) dx. \quad (18)$$

Thus, we identify

$$\nabla_{\delta\theta}\mathcal{J}_r = \nabla_{\delta\theta}\mathcal{J} + \beta \left(d_{\Omega_0}(x) + H \frac{1}{2} d_{\Omega_0}^2(x) \right). \quad (19)$$

Numerically, the level-set functions defined in section IV are used to approximate $d_{\Omega_0}(x)$. The parameter β controls how far the optimal shape can be from the initial guess and is determined *a posteriori*. Moreover a Sobolev gradient descent direction $\nabla_{\delta\theta}^{H^1}\mathcal{J}_r$, as in Protas et al. [23], is used in order ensure smooth shapes. The optimisation is performed by solving iteratively the direct and adjoint equations. The step size in the Sobolev Gradient direction is found using a backtracking Armijo algorithm [24].

IV. Numerical methods

A. Discrete model

We consider a finite element approximation. To avoid a remeshing procedure during the minimisation, an immersed boundary is taken into account by XFEM cut elements [25–27]. We consider the weak formulation for the direct problem (1) written compactly in matrix form

$$(\mathbf{K} + \mathbf{S})\mathbf{p} + ik\mathbf{D}\mathbf{p} - k^2\mathbf{M}\mathbf{p} = 2ike^{ikL}\mathbf{f}. \quad (20)$$

with \mathbf{p} the vector of the degrees of freedom associated with p . \mathbf{K} , \mathbf{M} , \mathbf{D} and \mathbf{f} are respectively the stiffness matrix, the mass matrix, the mass matrix on Γ_Z and unitray source term on Γ_Z . Boundary conditions in (1) are enforced by substituting $\frac{\partial p}{\partial n}$ in the contour terms. Cut elements can induce numerical oscillations due to ill-conditioning of the mass matrix when the boundary passes very close to a mesh node. Indeed, in that situation, the size of some elements can become very small. Then, a stabilisation term \mathbf{S} is added consistently with the one proposed by Burman [28].

Similarly, the adjoint problem (9) is

$$(\mathbf{K} + \mathbf{S})^*\lambda - ik^*\mathbf{D}^*\lambda - (k^*)^2\mathbf{M}^*\lambda = \frac{4}{R^2} \frac{e^{ikL}j(p, k)}{(e^{-ikL} + e^{ikL} - \bar{p})^2} \mathbf{f}, \quad (21)$$

with λ the vector of the degrees of freedom associated with λ .

B. Level-set transport

Let us consider a working bounded domain \mathcal{D} in which the open set $\Omega \subset \mathcal{D}$ is immersed. In practice, \mathcal{D} is meshed once for all. In order to locate the immersed boundary, we use a level-set function such that

$$\begin{cases} \psi = 0 & x \in \Gamma_\theta \cap \mathcal{D} \\ \psi > 0 & x \in \Omega \\ \psi < 0 & x \in (\mathcal{D} \setminus (\Omega \cup \Gamma_\theta)). \end{cases} \quad (22)$$

On Γ_θ , we have the outward normal direction $\mathbf{n} = -\frac{\nabla\psi}{|\nabla\psi|}$, and the curvature $H = \text{div}(\mathbf{n})$. To move the shape in the direction $\delta\theta$, the following transport equation is used

$$\frac{\partial\psi}{\partial t} + \mathbf{v} \cdot \nabla\psi = 0. \quad (23)$$

Since the shape is invariant with respect to a displacement tangential to the boundary, we consider only normal velocities as shape variations $\mathbf{v} = v \cdot \mathbf{n}$, that leads to the scalar relation

$$\frac{\partial\psi}{\partial t} + v|\nabla\psi| = 0. \quad (24)$$

We recall that the descent direction is

$$\mathbf{v} = \delta\theta \cdot \mathbf{n} = -\nabla_{\delta\theta}^{H^1} \mathcal{J}_r \cdot \mathbf{n}. \quad (25)$$

The transport equation (24) is solved implicitly with a Streamline Upwind Petrov Galerkin (SUPG) scheme [29].

Beside localising the shape boundary, another role of the level set is to give access to the signed distance function $d_{\Omega_0}(x)$. A way of doing that is to solve a pseudo-temporal equation [see for instance 3, 30] coupled with a diffusive term proposed by Li et al. [31] such that the steady solution of this equation is the distance to the iso-contour $\psi_0 = 0$, *i.e.* to Γ_θ . For this reason, we replace in (17) $d_{\Omega_0}(x)$ by $\psi - \psi_{ci}$, with ψ_{ci} the regularised level set at the initial condition. These quantities indeed correspond to $d_{\Omega_0}(x) = -\psi_0$ on Γ_θ , *i.e.* where they are evaluated. Moreover, the level-set can become stiff during the transport process. This effect can lead to inaccurate gradients computations. To cope this difficulty, few time steps of this pseudo-temporal equation are performed at each iteration of the optimisation.

V. Results

A. General settings

The domain considered has a cavity depth $D = 2.32$, a thickness $e = 0.11$, a hole diameter $d = 0.25$, a tube length $L = 5$ and a cell radius is $R = 0.5$. The Reynolds number is $Re_a = 1.85 \times 10^5$ and the Prandtl number is $Pr = 0.7$. The orders of magnitude of these parameters are representative of realistic values found for acoustic liners integrated in aircraft engines. The domain is discretised by 59352 $P2$ elements, leading to 117427 degrees of freedom. The target impedance is $Z_T = 1$, corresponding to a perfect absorption, over the frequency range $k \in [0.08 : 0.1]$.

B. Shape optimisation

The parameters used for the optimisation are the following. A tolerance of 10^{-6} on variations of J_r and of 10^{-3} on the L^2 norm of the gradient define the stopping criteria. The linesearch algorithm starts with an initial step of $\alpha_0 = 2 \times 10^{-3}$ with a relaxation parameter $\gamma = 0.5$ and an Armijo condition tolerance of $\epsilon_{\text{Armijo}} = 0.1$ such that the step is accepted if $\mathcal{J}_r^i - \mathcal{J}_r^{i+1} > \epsilon_{\text{Armijo}} \alpha_i \|\nabla \mathcal{J}_r^i\|_{H_1}$ with α_i the optimisation step. In order to highlight the effect of the regularisation by penalising the distance to the initial shape, various values of the associated parameter are chosen $\beta = \{10^{-1}, 2.10^{-1}, 5.10^{-1}, 2.10^0\}$.

Convergence of the optimisation problem is illustrated in figure 4 by the cost functional \mathcal{J}_r during the iterations for different values of β . As it can be expected in a Tikhonov regularisation, increasing the regularisation parameter β accelerates the convergence toward a larger value of cost functional \mathcal{J}_r . The optimal shapes obtained are displayed in figure 3. As expected, the shape moves away from the initial shape as β is decreased.

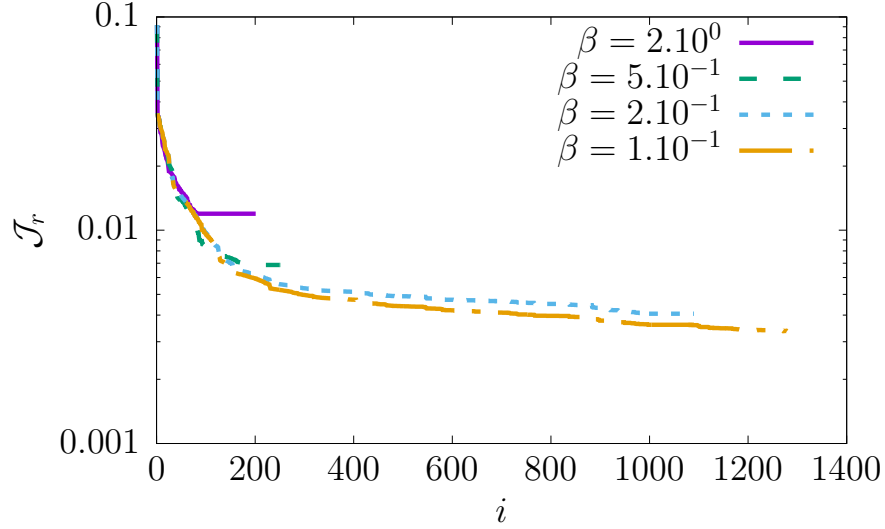


Fig. 2 Cost functional \mathcal{J}_r as a function of the iteration i during the convergence of the optimisation problem, for various values of wall-distance regularisation parameter β .

The resistance, reactance and absorption coefficients are displayed in figure 4. We compare the situation where no immersed wall are considered, the initial guess and the optimal shapes. The resonance frequency can be visualised when the reactance vanishes. We can see that all the optimisations quickly bring the resonance frequency in the optimisation frequency range. The shape with no immersed wall has a very low resistance, while the initial guess is too resistive. Relaxing the regularisation β allows to bring the resistances closer to one, which leads to high absorptions. We can see that an almost perfect absorption is reached for $\beta \leq 5.10^{-1}$ in the desired frequency range.

As can be seen in figure 3, between $\beta = 5.10^{-1}$ and $\beta = 2.10^{-1}$, a quick change of shape brings it far from the initial guess and a further decrease of β leads to spurious oscillations of the shape. This illustrates the necessity to regularise this optimisation problem. Looking at the acoustic performance, a regularisation parameter of $\beta = 5.10^{-1}$ appears in our case to be a good compromise. The procedure is classically quantified by L-curve method [32]. This consists in plotting the performance cost functional \mathcal{J} with respect to penalty $\mathcal{J}_d = \frac{1}{2} \int_{\Gamma_\theta} d_{\Omega_0}^2(x) dx$. This curve typically has a “L” shape, and a fair compromise is to select a value of β in the corner of this curve. Unfortunately the curve (not shown

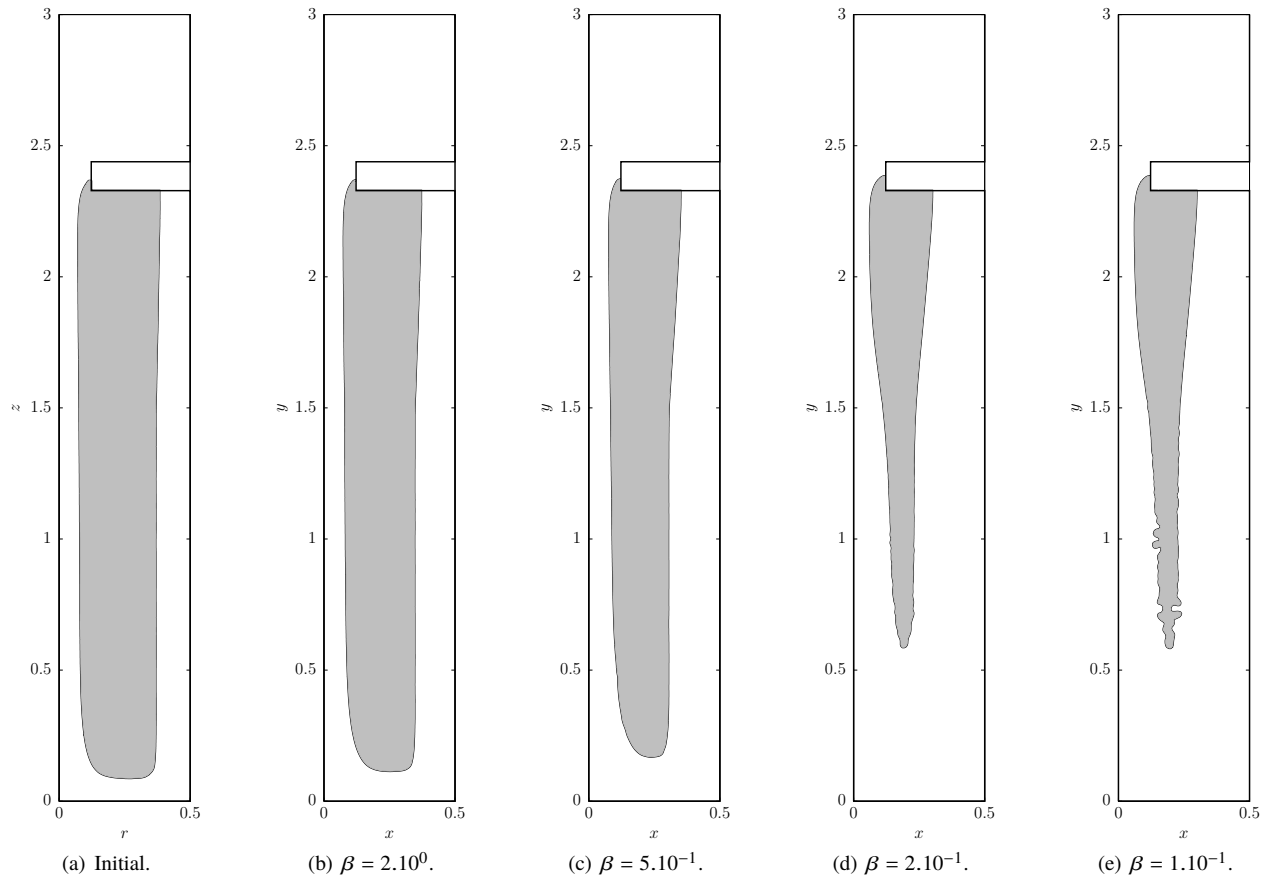
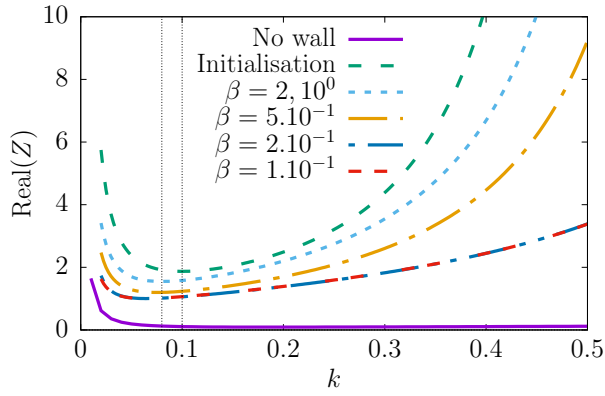
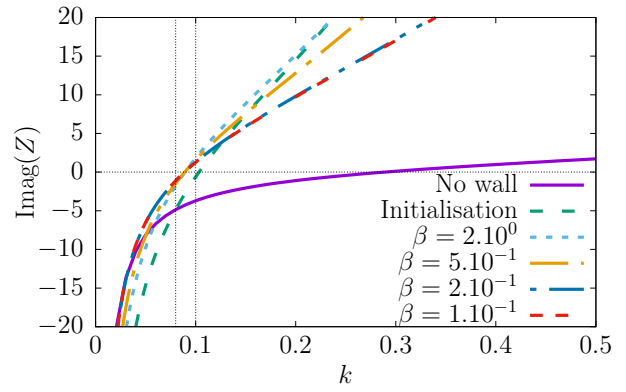


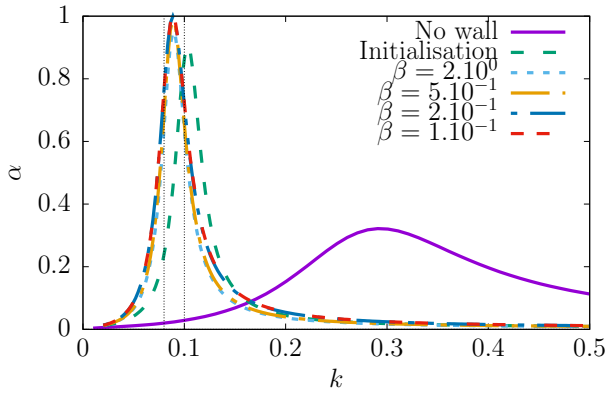
Fig. 3 Optimal cavity shapes for different values of the regularisation parameter β . The gray zones correspond to the immersed body.



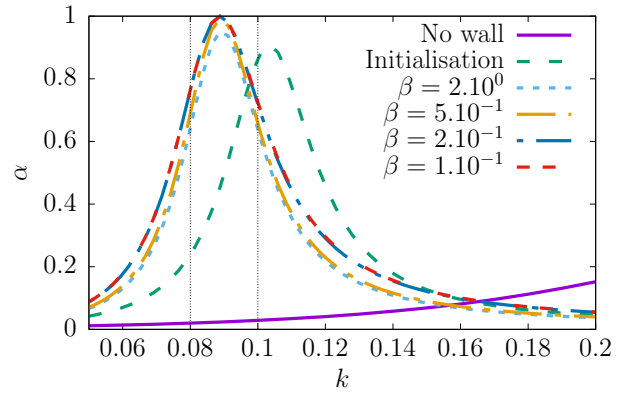
(a) Resistance.



(b) Reactance.



(c) Absorption.



(d) Zoom of the absorption graph.

Fig. 4 Performance of the optimal shapes for different values of the regularisation parameter β .

here) is a straight line in our case, suggesting to decrease even more the regularisation parameter β . This is obviously not a reasonable choice with regard to the regularity of the shape figure 3(e). A penalty based on the total variation of the shape would certainly produce a L-curve, but it is out of the scope of the present paper.

VI. Conclusion

In this paper we have demonstrated the possibility of using shape optimisation for the design of absorbing treatments by impedance matching. The use of a model for viscous losses as an equivalent boundary condition allows to use the Helmholtz equation, that is computationally more tractable than employing the full linearised Navier-Stokes equations. The price to pay is the implementation of boundary terms in the shape derivative that involve the wall curvature and second derivatives in space. In that context, the use of the Sobolev gradient as a descent direction improves significantly the regularity of the optimisation problem. In addition, a Tikhonov regularisation allows to penalise the distance of the optimal shape to an initial guess. This improves the well-posedness of the problem and gives to the designer a degree of control to obtain shapes that can be manufactured in the context of a local optimisation. For the numerical implementation, a XFEM numerical method has been used where the immersed boundary is tracked by a level set function. This methodology has been employed to optimise the cavity shape of a liner, leading to an almost perfect absorption at a frequency range where standard treatments are inefficient.

Acknowledgements

The authors gratefully acknowledge the financial support of the Chaire Industrielle MACIA (ANR-16-CHIN-0002) provided by the Safran Group and the Agence Nationale de la Recherche.

Appendix

The Lagrangian (8) is differentiated with respect to each variable. This appendix details the calculations.

Derivative with respect to λ

$$(\nabla_{\lambda} \mathcal{L}, \delta \lambda) = 0 \quad (26)$$

leads to

$$\Delta p + k^2 p = 0. \quad (27)$$

Boundary conditions will be enforced later implicitly by using them during the calculation.

Derivative with respect to p :

$$(\nabla_p \mathcal{L}, \delta p) = (\nabla_p \mathcal{J}, \delta p) - \int_{k_1}^{k_2} \text{real} \left[\left(\lambda, \Delta \delta p + k^2 \delta p \right) \right] dk \quad (28)$$

We expand each term separately.

$$\begin{aligned} (\nabla_p \mathcal{J}, \delta p) &= \int_{k_1}^{k_2} \text{real} \left[j^*(p, k) \frac{\partial j(p, k)}{\partial p} \delta p \right] dk \\ &= \int_{k_1}^{k_2} \text{real} \left[\left(\frac{\frac{2}{R^2} \int_{\Gamma_Z} \delta p dl}{e^{-ikL} + e^{ikL} - \bar{p}} - \frac{(e^{-ikL} - e^{ikL} + \bar{p}) \left(-\frac{2}{R^2} \int_{\Gamma_Z} \delta p dl \right)}{(e^{-ikL} + e^{ikL} - \bar{p})^2} \right) j^*(p, k) \right] dk \\ &= \int_{k_1}^{k_2} \text{real} \left[\int_{\Gamma_Z} \left(\frac{\frac{4}{R^2} e^{ikL} j(p, k)}{\left((e^{-ikL} + e^{ikL} - \bar{p})^2 \right)^*} \right) \delta p dl \right] dk. \end{aligned} \quad (29)$$

Besides, we have

$$\begin{aligned}
& - \int_{k_1}^{k_2} \text{real} \left[\left(\lambda, \Delta \delta p + k^2 \delta p \right) dk \right] \\
& = - \int_{k_1}^{k_2} \text{real} \left[\left(\Delta \lambda + (k^*)^2 \lambda, \delta p \right) - \int_{\Gamma_w} (\nabla \lambda^* \cdot \mathbf{n}) \delta p dl + \int_{\Gamma_w} \lambda^* (\nabla \delta p \cdot \mathbf{n}) dl \right. \\
& \quad \left. - \int_{\Gamma_Z} (\nabla \lambda^* \cdot \mathbf{n}) \delta p dl + \int_{\Gamma_Z} \lambda^* (\nabla \delta p \cdot \mathbf{n}) dl - \int_{\Gamma_s} (\nabla \lambda^* \cdot \mathbf{n}) \delta p dl + \int_{\Gamma_s} \lambda^* (\nabla \delta p \cdot \mathbf{n}) dl \right] dk \quad (30) \\
& = - \int_{k_1}^{k_2} \text{real} \left[\left(\Delta \lambda + (k^*)^2 \lambda, \delta p \right) + \int_{\Gamma_Z} -(\nabla \lambda^* \cdot \mathbf{n}) \delta p + (ik^* \lambda)^* \delta p dl + \int_{\Gamma_s} -(\nabla \lambda^* \cdot \mathbf{n}) \delta p dl \right. \\
& \quad \left. + \int_{\Gamma_w} \left(-(\nabla \lambda \cdot \mathbf{n}) + \delta_v \frac{-i-1}{2} \Delta_T \lambda - \delta_T (k^*)^2 \frac{(-i-1)(\gamma-1)}{2} \lambda \right)^* \delta p dl \right] dk.
\end{aligned}$$

We deduce the adjoint equation

$$\begin{cases}
\Delta \lambda + (k^*)^2 \lambda = 0 & x \in \Omega \\
\nabla \lambda \cdot \mathbf{n} + \delta_v \frac{i+1}{2} \Delta_T \lambda - \delta_T (k^*)^2 \frac{(i+1)(\gamma-1)}{2} \lambda = 0 & x \in \Gamma_w \\
\nabla \lambda \cdot \mathbf{n} - ik^* \lambda = \frac{4}{R^2} \frac{e^{ikL} j(p, k)}{(e^{-ikL} + e^{ikL} - \bar{p})^2} & x \in \Gamma_Z \\
\nabla \lambda \cdot \mathbf{n} = 0 & x \in \Gamma_s.
\end{cases} \quad (31)$$

References

- [1] Díaz, A. R., and Kikuchi, N., “Solutions to shape and topology eigenvalue optimization problems using a homogenization method,” *International Journal for Numerical Methods in Engineering*, Vol. 35, No. 7, 1992, pp. 1487–1502.
- [2] Ma, Z.-D., Cheng, H.-C., and Kikuchi, N., “Structural design for obtaining desired eigenfrequencies by using the topology and shape optimization method,” *Computing Systems in Engineering*, Vol. 5, No. 1, 1994, pp. 77–89.
- [3] Allaire, G., Jouve, F., and Toader, A.-M., “Structural optimization using sensitivity analysis and a level-set method,” *Journal of computational physics*, Vol. 194, No. 1, 2004, pp. 363–393.
- [4] Allaire, G., De Gournay, F., Jouve, F., and Toader, A.-M., “Structural optimization using topological and shape sensitivity via a level set method,” *Control and Cybernetics*, Vol. 34, No. 1, 2005, p. 59.
- [5] Achtziger, W., and Kočvara, M., “Structural topology optimization with eigenvalues,” *SIAM Journal on Optimization*, Vol. 18, No. 4, 2007, pp. 1129–1164.
- [6] Jameson, A., “Aerodynamic shape optimization using the adjoint method,” *Lectures at the Von Karman Institute, Brussels*, 2003.
- [7] Sonntag, M., Schmidt, S., and Gauger, N. R., “Shape derivatives for the compressible Navier–Stokes equations in variational form,” *Journal of Computational and Applied Mathematics*, Vol. 296, 2016, pp. 334–351.
- [8] Jensen, J. S., and Sigmund, O., “Topology optimization of photonic crystal structures: a high-bandwidth low-loss T-junction waveguide,” *Journal of Optical Soscity of America B*, Vol. 22, No. 6, 2005, pp. 1191–1198.
- [9] Wang, F., Jensen, J. S., and Sigmund, O., “Robust topology optimization of photonic crystal waveguides with tailored dispersion properties,” *Optical Society of America. Journal B: Optical Physics*, Vol. 28, No. 3, 2011, pp. 387–397.
- [10] Bångtsson, E., Noreland, D., and Berggren, M., “Shape optimization of an acoustic horn,” *Computer Methods in Applied Mechanics and Engineering*, Vol. 192, No. 11-12, 2003, pp. 1533–1571.
- [11] Udawalpola, R., and Berggren, M., “Optimization of an acoustic horn with respect to efficiency and directivity,” *International Journal for Numerical Methods in Engineering*, Vol. 73, No. 11, 2008, pp. 1571–1606.

- [12] Wadbro, E., Udawalpola, R., and Berggren, M., “Shape and topology optimization of an acoustic horn–lens combination,” *Journal of Computational and Applied Mathematics*, Vol. 234, No. 6, 2010, pp. 1781–1787.
- [13] Udawalpola, R., Wadbro, E., and Berggren, M., “Optimization of a variable mouth acoustic horn,” *International Journal for Numerical Methods in Engineering*, Vol. 85, No. 5, 2011, pp. 591–606.
- [14] Bernland, A., Wadbro, E., and Berggren, M., “Acoustic shape optimization using cut finite elements,” *International Journal for Numerical Methods in Engineering*, Vol. 113, No. 3, 2018, pp. 432–449.
- [15] Caeiro, F., Sovardi, C., Förner, K., and Polifke, W., “Shape optimization of a Helmholtz resonator using an adjoint method,” *International Journal of Spray and Combustion Dynamics*, Vol. 9, No. 4, 2017, pp. 394–408.
- [16] Dühring, M. B., Jensen, J. S., and Sigmund, O., “Acoustic design by topology optimization,” *Journal of Sound and Vibration*, Vol. 317, No. 3-5, 2008, pp. 557–575.
- [17] Desai, J., Faure, A., Michailidis, G., Parry, G., and Estevez, R., “Topology optimization in acoustics and elasto-acoustics via a level-set method,” *Journal of Sound and Vibration*, Vol. 420, 2018, pp. 73–103.
- [18] Berggren, M., Bernland, A., and Noreland, D., “Acoustic boundary layers as boundary conditions,” *Journal of Computational Physics*, Vol. 371, 2018, pp. 633 – 650.
- [19] Bossart, R., Joly, N., and Bruneau, M., “Hybrid numerical and analytical solutions for acoustic boundary problems in thermo-viscous fluids,” *Journal of Sound and Vibration*, Vol. 263, No. 1, 2003, pp. 69 – 84.
- [20] Andersen, P. R., Henríquez, V. C., and Aage, N., “Shape optimization of micro-acoustic devices including viscous and thermal losses,” *Journal of Sound and Vibration*, 2019.
- [21] Allaire, G., Jouve, F., and Michailidis, G., “Thickness control in structural optimization via a level set method,” *Structural and Multidisciplinary Optimization*, Vol. 53, No. 6, 2016, pp. 1349–1382.
- [22] Tikhonov, A. N., and Arsenin, V. Y., *Solution of ill-posed problems*, Winston & Sons, 1977.
- [23] Protas, B., Bewley, T. R., and Hagen, G., “A computational framework for the regularization of adjoint analysis in multiscale PDE systems,” *Journal of Computational Physics*, Vol. 195, No. 1, 2004, pp. 49–89.
- [24] Armijo, L., “Minimization of functions having Lipschitz continuous first partial derivatives,” *Pacific Journal of Mathematics*, Vol. 16, No. 1, 1966, pp. 1–3.
- [25] Moës, N., Dolbow, J., and Belytschko, T., “A finite element method for crack growth without remeshing,” *International Journal for Numerical Methods in Engineering*, Vol. 46, No. 1, 1999, pp. 131–150.
- [26] Legrain, G., Chevaugeon, N., and Dréau, K., “High order X-FEM and levelsets for complex microstructures: uncoupling geometry and approximation,” *Computer Methods in Applied Mechanics and Engineering*, Vol. 241, 2012, pp. 172–189.
- [27] Burman, E., Claus, S., Hansbo, P., Larson, M. G., and Massing, A., “CutFEM: discretizing geometry and partial differential equations,” *International Journal for Numerical Methods in Engineering*, Vol. 104, No. 7, 2015, pp. 472–501.
- [28] Burman, E., “Ghost penalty,” *Comptes Rendus Mathématique*, Vol. 348, No. 21-22, 2010, pp. 1217–1220.
- [29] Donea, J., and Huerta, A., *Finite element methods for flow problems*, John Wiley & Sons, 2003.
- [30] Osher, S., and Fedkiw, R. P., “Level set methods: an overview and some recent results,” *Journal of Computational physics*, Vol. 169, No. 2, 2001, pp. 463–502.
- [31] Li, C., Xu, C., Gui, C., and Fox, M. D., “Distance regularized level set evolution and its application to image segmentation,” *IEEE Transactions on Image Processing*, Vol. 19, No. 12, 2010, pp. 3243–3254.
- [32] Hansen, P. C., “Analysis of discrete ill-posed problems by means of the L-curve,” *SIAM review*, Vol. 34, No. 4, 1992, pp. 561–580.